electricity

MDPI

Article

Transient Stability Assessment of a 9-Bus Power System with High Solar PV Penetration: An IEEE Benchmark Case Study

Marvens Jean Pierre [1], Emmanuel Hernández-Mayoral [1,*], Oscar Alfredo Jaramillo Salgado [1], Manuel Madrigal-Martínez [2], Reynaldo Iracheta-Cortez [3], Jorge Sanchez-Jaime [4] and Gregorio Martínez-Reyes [3]

1 Instituto de Energías Renovables, Universidad Nacional Autónoma de México (UNAM), Priv. Xochicalco s/n, Temixco 62580, Morelos, Mexico; majepi@ier.unam.mx (M.J.P.); ojs@ier.unam.mx (O.A.J.S.)
2 Instituto Tecnológico de Morelia, Tecnológico Nacional de México, Av. Tecnológico 1500, Morelia 58120, Michoacán, Mexico; manuelmadrigalmtz@gmail.com
3 Graduate Studies Division, Isthmus University, Tehuantepec 70760, Oaxaca, Mexico; irachetacortez97@gmail.com (R.I.-C.); mrgregorio23@gmail.com (G.M.-R.)
4 Instituto Tecnológico de Toluca, Tecnológico Nacional de México, Metepec 52149, Estado de México, Mexico; jsanchezj@toluca.tecnm.mx
* Correspondence: emhema@ier.unam.mx

Abstract

This study examines the impact of increasing photovoltaic (PV) penetration on the transient stability of the IEEE 9-bus power system. Synchronous machines are modeled with standard subtransient dynamics, while PV units are represented as current-limited grid-following inverters. Transient stability is assessed through the Critical Clearing Time (CCT) and the post-fault dynamic behavior, obtained from time-domain simulations carried out in MATLAB/Simulink® R2023b. Two permanent three-phase faults are considered: a primary contingency on line 7–5 and a secondary contingency on line 9–6, introduced to assess the robustness of the observed trends across different fault locations. The results show an increase in CCT as PV generation progressively replaces the active power supplied by synchronous machines, whose inertia is therefore maintained: from 210 ms (0% PV) to 440 ms (25%)/1080 ms (40%) at bus 5, 410 ms (25%)/1130 ms (40%) and 290 ms (25%)/650 ms (40%) at buses 6 and 8, respectively, demonstrating that the penetration site is a key factor for system stability. For distributed penetration among the three buses, CCT values of 340 ms (25%) and 1020 ms (40%) highlight the significant influence of PV placement at bus 8. The fault on line 9–6 consistently yields higher CCT values across all scenarios, confirming the robustness of these trends independently of fault location. Although an overall increase in CCT was observed, higher PV penetration also led to more pronounced oscillations and operability issues after the fault. In particular, 75% of the penetration scenarios under the fault on line 9–6 do not meet the active power recovery requirements of IEEE 1547-2018 and IEEE 2800-2022, a result more severe than that observed for the fault on line 7–5. These results underscore that a higher CCT does not guarantee operational compliance, and that stability-oriented control strategies—such as grid-forming operation, fast active power support, and dynamic voltage control—remain essential. They also suggest that planning practices should favor interconnections electrically closer to the slack generator. Overall, a high PV penetration level—modifying only the operating point of synchronous machines—allows longer fault durations to be tolerated; however, appropriate siting of PV units and the adoption of advanced inverter controls could mitigate the observed oscillations and post-fault operability challenges.

Check for updates

Academic Editor: Murilo Eduardo Casteroba Bento

Received: 9 April 2026
Revised: 12 May 2026
Accepted: 15 May 2026
Published: 20 May 2026

Copyright: © 2026 by the authors. Licensee MDPI, Basel, Switzerland. This article is an open access article distributed under the terms and conditions of the Creative Commons Attribution (CC BY) license.

Keywords: critical clearing time (CCT); electrical power system; PV penetration; transient stability; IEEE 9-bus power system

1. Introduction

Renewable energy sources (RESs) are integrated into conventional electrical power systems (EPSs) to solve issues like fossil fuel shortages, rising energy demand, and environmental pollution [1]. Among the alternative RESs, solar PV systems are now a well-established option due to their simple design and low capital and operational costs. It is also notable that, worldwide, total PV capacity has increased at an average annual rate of 55% [2]. These factors have made PV technology an attractive option for power generation and a central focus of ongoing research in modern power systems.

PV systems can generally be classified into two main categories, namely isolated and connected to the grid, the latter being the ones that have been widely adopted. Although PV renewable energy brings clear environmental advantages, its integration also alters the operational and dynamic characteristics of electrical power systems compared to conventional grids [3]. Unlike synchronous generators, inverter-based renewable units do not store kinetic energy in a rotating mass and therefore cannot inherently contribute to the inertial response of the system. Their interaction with the grid occurs through power-electronic converters, whose current and control limitations reduce the system's effective inertia and weaken the synchronizing torque. As a consequence, the ability of the grid to withstand and mitigate disturbances can be significantly affected, and the transient stability margin may be compromised [4].

The need to integrate renewable energy sources with high penetration, driven by the energy transition and the major advances in power electronics, has become a central research topic due to the new grid configurations and the different responses they exhibit under various disturbances. Numerous studies have been conducted in this field and have highlighted both positive and negative effects associated with high PV penetration in EPSs.

In the study presented in [5], the authors reported that, due to the stochastic nature of PV systems, issues such as voltage and frequency fluctuations, active power variations, reactive power flow changes, and degraded system dynamics may arise as a consequence of irradiation variations caused by the rapid and constant movement of clouds. Factors such as the size and location of PV systems, whether they are distributed or concentrated, the availability of sufficient reserves in the system, the displacement of conventional generators by PV production, the reactive power compensation method, and the control loops influence the impact of PV penetration on the EPS with respect to voltage stability, frequency stability, and transient stability [6].

Conversely, the authors in [7] observed that high PV penetration affects the angle and frequency stability of the transmission system. In [8], the transient stability of large-scale PV systems integrated into the Ontario grid was examined. Their results indicate that transient stability improves more with distributed PV penetration than with concentrated PV. The effect of PV systems installed on residential rooftops was analyzed in [9] with respect to the transient stability of an interconnected grid in the western United States. The findings suggest that increasing PV penetration deteriorates transient stability due to the reduction in system inertia; however, when faults occur in less critical locations, transient stability can improve. Finally, the authors investigated the effect of different levels of PV penetration on rotor angle stability in the standard IEEE 9-bus test system, described in [10], and found that increasing PV penetration improves transient stability when the synchronous generator is not replaced. When it is replaced, system stability decreases.

They ultimately concluded that the key factors influencing transient stability in an EPS are the PV penetration level, the fault clearing time, and the fault location.

In summary, this literature review shows that the behavior of the power system under high PV penetration depends strongly on how this penetration is implemented. An improvement in transient stability is generally observed when the synchronous generator is not replaced and synchronous inertia remains constant, highlighting the complexity of understanding these systems and the need for further research. Despite the variety of studies in the field, few investigations focus on the post-fault dynamic behavior of systems, particularly in scenarios where PV penetration does not reduce transient angular stability margins. Most previous works primarily evaluate stability through indicators such as the CCT or rotor-angle response, while less attention is given to post-fault operational performance and compliance with modern grid-code requirements such as IEEE 1547-2018 [11] and IEEE 2800-2022 [12]. However, an increase in CCT does not necessarily imply satisfactory post-fault active power recovery or acceptable dynamic operability. Therefore, evaluating both transient stability margins and post-fault dynamic behavior becomes essential for understanding the practical implications of high PV penetration.

This article conducts simulations to evaluate the transient stability of the IEEE 9-bus system under different levels of PV penetration. The main objective is to determine the Critical Clearing Time (CCT), considering the geographical location of the penetrations and the various penetration typologies. Here, penetration refers to the active power supplied by PV systems that is incorporated into the EPS.

More specifically, the work comprises the following:

- Developing a detailed simulation model of the IEEE 9-bus system for transient stability studies, comprising three synchronous generators and current-limited grid-following inverters representing PV units connected at buses 5, 6, and 8. PV penetration levels of 25% and 40% were implemented using MATLAB /Simulink® R2023b.
- Considering permanent three-phase faults on lines 7–5 and 9–6 of the grid. The computation of the CCT and the analysis of the post-fault dynamic behavior were carried out for each level of PV penetration, including both distributed and concentrated penetration scenarios, in which the synchronous generators are not replaced (constant synchronous inertia). The fault on line 9–6 was introduced as a secondary contingency to assess the robustness of the observed trends across different fault locations.

The main scientific contributions of this work can be summarized as follows:

- The use of CCT as a quantitative indicator to assess the impact of high PV penetration on transient stability, allowing a systematic comparison of different penetration levels, penetration locations, and topological configurations within a benchmark power system.
- A detailed analysis of the influence of PV penetration location on system robustness, identifying critical buses where PV integration leads to lower stability margins and increased vulnerability to severe disturbances.
- An explicit investigation of post-fault operational behavior, including rotor angle oscillations and active power recovery, enabling the assessment of system operability with respect to technical requirements imposed by IEEE 1547-2018 and IEEE 2800-2022.
- A benchmark-based analytical methodology that highlights fundamental transient stability mechanisms under high PV penetration while intentionally isolating the effects of penetration level, location, and topology by maintaining constant synchronous inertia.

Although the study is conducted on a reduced IEEE 9-bus benchmark system and the results should be interpreted as indicative trends rather than directly transferable

operational rules, the IEEE 9-bus system remains widely used in transient stability research due to its ability to reproduce the fundamental electromechanical interactions of power systems under controlled conditions. Its simplified structure facilitates the isolation of key variables such as PV penetration level, penetration location, and fault contingency, while preserving sufficient dynamic complexity for rotor-angle and post-fault response analysis. Furthermore, its continued use in recent PV integration and inverter-based stability studies enables direct comparison with the previous literature [10,13,14]. Therefore, the findings provide valuable insights for power system planners and researchers, particularly regarding the identification of critical integration scenarios and the importance of jointly considering transient stability margins and post-fault operability when integrating large shares of converter-based renewable generation.

2. Materials and Methods

2.1. Transient Stability Criterion

The dynamics in EPSs can be classified according to different time scales, including electromagnetic and electromechanical dynamics, whereas steady-state represents a static operating condition rather than a dynamic regime. Small, gradual changes in the EPS are considered minor disturbances, and studying stability within this domain is known as small-signal stability. Large disturbances, such as the disconnection of large loads or generators, the rupture of transmission lines or link lines, and short circuits, relate to the concept of transient stability, which is defined as the ability of the EPS to remain synchronized under large disturbances. During such events, transient stability analysis helps determine the deviation behavior of the rotor angle. If these disturbances are not removed within a specified time, they can cause generators to lose synchronism, potentially leading to the disconnection of the entire system.

To study transient stability, various indicators can be examined, including rotor velocity deviation, rotor angle, frequency, voltage at the generator terminals, and the CCT of faults [15]. The CCT is defined as the maximum time available to eliminate a fault while maintaining system stability [13]. A higher CCT means more time to clear faults, making the system safer. An important factor in stability studies is the power dynamics over different time scales. For conventional EPSs dominated by synchronous generators, electromechanical dynamics typically evolve over a time frame of several seconds. In contrast, renewable energy sources interfaced through power electronic converters exhibit faster dynamics, often occurring over shorter time scales [16]. Achieving transient stability in an EPS requires generators to remain synchronized, keeping the stability indicators within acceptable limits. However, the CCT value depends on factors such as generator size, inertia, dispatch conditions, line impedances, grid topology, fault location, and other transient stability-related aspects. Additionally, weather conditions may indirectly influence transient stability through their impact on renewable generation and load profiles.

2.2. Main Transient Stability Assessment Methods

Transient stability assessment can be conducted using different analytical approaches, depending on the nature of the disturbance, the level of model detail, and the objectives of the study. Classical power system literature distinguishes three main categories of methods: time-domain simulations, eigenvalue-based (small-signal) analysis, and energy-based approaches [17,18].

Time-domain simulation is the most widely used method for transient stability analysis under large disturbances, such as three-phase short circuits, generator outages, and line tripping events. This approach consists of numerically solving the nonlinear swing

equations and grid algebraic equations to directly observe rotor angle trajectories and stability margins in the time domain [19].

Eigenvalue analysis, derived from the linearized system Jacobian matrix around an operating point, is primarily used for small-signal stability studies. While this method provides valuable insight into oscillatory modes, damping characteristics, and system sensitivity, it is inherently limited to small perturbations and cannot accurately represent nonlinear behavior under severe faults [17].

Energy-based methods, such as the transient energy function approach, evaluate system stability by comparing the system kinetic and potential energy during a disturbance. These methods offer analytical insight into stability margins but require simplifying assumptions and are generally less suitable for systems with complex controls and converter-interfaced generation [18].

The main methods for assessing transient stability, their advantages and limitations are summarized in Table 1.

In this paper, transient stability is assessed using time-domain simulation of the nonlinear swing equation, as this approach is particularly suited for large disturbances and allows direct evaluation of CCT and post-fault dynamic behavior.

Table 1. Comparison of main transient stability assessment methods based on classical power system literature.

Method	Main Advantages	Main Limitations
Time-domain simulation	- Captures full nonlinear system behavior - Suitable for large disturbances - Direct evaluation of rotor angles and CCT	- Computationally intensive - Requires detailed system models
Eigenvalue analysis	- Provides modal and damping information - Computationally efficient - Useful for control design	- Valid only for small disturbances - Based on linearized models
Energy-based methods	- Provides analytical insight into stability margins - Less dependent on time-domain simulation	- Requires simplifying assumptions - Limited applicability with complex controls

2.3. Dynamic Modeling of Synchronous Generators

After exposing the EPS to a three-phase (3ϕ) fault, the transient stability is analyzed using the oscillation equation described in (1), which represents the classical swing equation of a synchronous generator and governs the electromechanical dynamics of the rotor.

$$\frac{H}{\pi f_0}\frac{d^2\delta}{dt^2} = P_m - P_e \tag{1}$$

This equation describes the balance between the mechanical power input and the electrical power output, where any mismatch between P_m and P_e results in rotor acceleration or deceleration. Here, H (in seconds) is the inertia constant, defined as the ratio of the kinetic energy stored in the rotating masses of the synchronous generator at rated speed to its rated apparent power. More specifically, H is given by the ratio between the kinetic energy W_K [MJ] at nominal speed and the machine rating S_B [MVA]. f_0 [Hz] is the system frequency, δ [rad] is the rotor angular displacement, P_m [p.u.] is the mechanical power of the prime mover, and P_e [p.u.] is the electrical power delivered. When δ is expressed in degrees, the equation becomes:

$$\frac{H}{180\, f_0}\frac{d^2\delta}{dt^2} = P_m - P_e \tag{2}$$

After the EPS experiences a disturbance, the transient stability is analyzed by solving the nonlinear oscillation equation within 3 to 5 s (where $P_e = P_m$). The electrical power produced is then calculated as:

$$P_e = \frac{|E||V|}{X} \sin \delta \tag{3}$$

where E is the constant internal voltage behind the synchronous reactance (per unit), V is the load voltage of the infinite bus (per unit), and X is the steady-state reactance between the generator and the bus. From the curve of the angular displacement of power, shown in Figure 1, the maximum power delivered occurs at $\delta = 90°$, as indicated in Equation (4).

$$P_{\max} = \frac{|E||V|}{X} \tag{4}$$

Note that when $\delta < 90°$, the EPS is stable, while if $\delta > 90°$, the EPS is unstable. At $\delta = 90°$, the generator is considered marginally stable, so any further increase in the angle makes the EPS unstable.

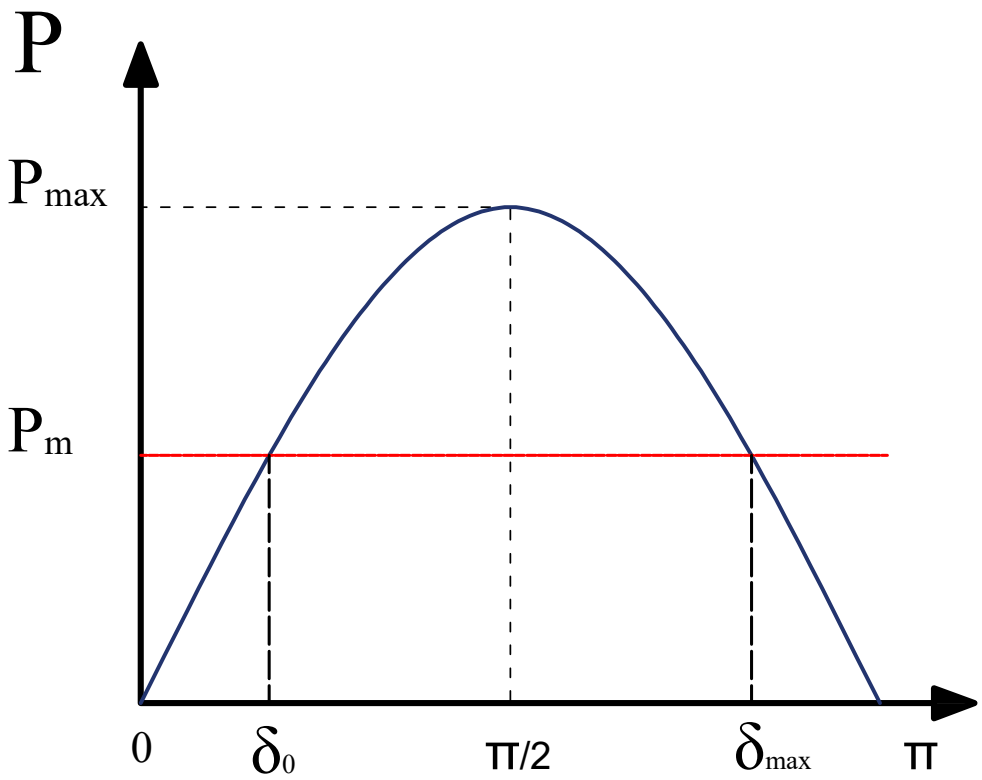


Figure 1. Power angular displacement curve for typical EPS.

The equation described in (1) allows us to study the rotor angle behavior of a single generator; however, the system used in this research is a multi-machine system consisting of three generators supplying three loads. For a multi-machine system composed of N generators, N swing equations are defined as in Equation (5), with the electrical power of machine i given by Equation (6). The system therefore contains N solutions $\delta(t) = \{\delta_1(t), \delta_2(t), \delta_3(t), \ldots, \delta_n(t)\}$ that make it possible to determine the transient stability of the multi-machine system. Due to their complexity, numerical methods are often used to solve these equations.

$$\frac{2H_i}{\omega_s} \frac{d^2\delta_i}{dt^2} = P_{\text{mec},i} - P_{\text{elec},i} \qquad i = 1, 2, \ldots, N \tag{5}$$

$$P_{\text{elec},i} = \sum_{\substack{j=1 \\ j\neq i}}^{N} \left|E_i'\right|\left|E_j'\right|\left|Y_{ij}^{\text{redu}}\right| \cos\left(\theta_{ij} + \delta_j - \delta_i\right) \tag{6}$$

2.4. Modeling of the PV Systems

A PV system consists of cells connected in series that form a module. Different models are used for PV cells to produce accurate results [20]. Figure 2 shows the equivalent circuit of a diode model of a PV cell.

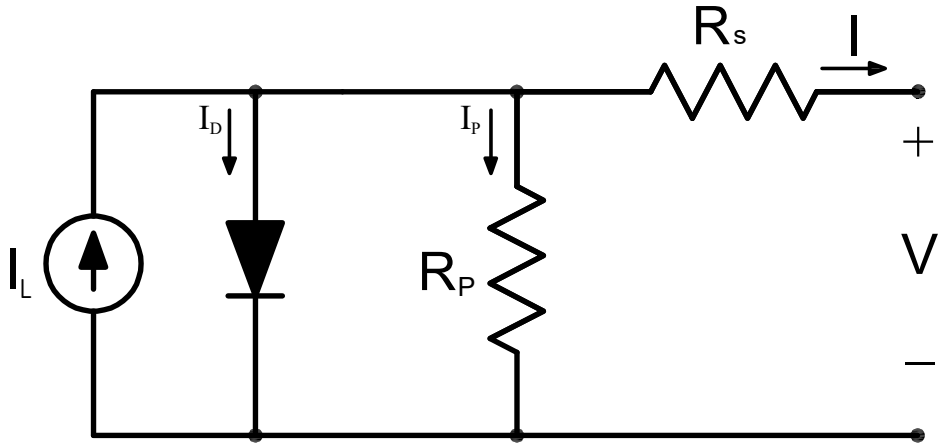


Figure 2. Equivalent electrical circuit of a typical (PV) cell (single-diode model).

Applying basic electrical engineering techniques, such as Kirchhoff's current law (KCL) and other methods detailed in [21], the output current of the PV cell, denoted by I, is determined as follows:

$$I = I_L - I_D - I_P \tag{7}$$

$$I_D = I_0\left[\exp\left(\frac{V + IR_s}{nV_T}\right) - 1\right] \tag{8}$$

$$I_P = \frac{V + IR_s}{R_P} \tag{9}$$

$$V_T = \frac{kT_C}{q} \tag{10}$$

where I_L is the current generated in the cell due to solar irradiance, I_D is the diode current governed by the Shockley equation shown in (8), and I_P is the current representing cell losses as expressed in (9). I_0 is the diode saturation current, n is the diode ideality factor, R_s and R_P are the series and parallel resistances used in the diode equivalent circuit, respectively. V_T is the thermal voltage defined in (10), k is the Boltzmann constant (1.381×10^{-23} J/K), T_C is the cell temperature, and q is the electron charge.

Therefore, Equation (7) becomes:

$$I_M = I_L - I_0\left[\exp\left(\frac{V_M + I_M N_S R_S}{nN_S V_T}\right) - 1\right] - \frac{V_M + I_M N_S R_S}{N_S R_P} \tag{11}$$

where V_M and I_M represent the module voltage and current, respectively; $V_M = N_S \times V_{\text{cell}}$, $I_M = I_{\text{cell}}$, and N_S denotes the number of cells connected in series in the PV module.

In this study, uniform irradiance and a consistent temperature are assumed for all cells in the modules and arrays. It is important to note that under fault conditions, PV systems behave differently from synchronous generators in conventional EPSs. Due to the presence of interface inverters that connect PV systems (which generate DC) to loads (which require AC), their short-circuit currents are typically below 150% of the nominal

current [22]. This is because inverters are equipped with modern protective current limiters designed to prevent high short-circuit currents and protect semiconductor switches.

To model the PV system, PV modules—each composed of multiple PV cells—are arranged in series and parallel to form a PV string with a nominal capacity of 6 MWp. This configuration is capable of delivering up to 6 MVA to the 230 kV three-phase grid through power electronic converters. To extract the maximum power from the PV array, grid-following inverters are placed at the output of each string. A Perturbation and Observation (P&O) algorithm is used as the direct control strategy for the maximum power point tracking (MPPT) while operating in unity power factor mode (PF = 1) and does not incorporate dedicated fault-reactive support or voltage-support control strategies during disturbances. Consequently, the inverter contribution to reactive power support under fault conditions is expected to remain limited in the present study.

This modeling choice is consistent with IEEE 1547-2018, which specifies unity power factor as the default operating mode for distributed energy resources unless otherwise required by the grid operator. Furthermore, IEEE 2800-2022 considers inverter-based resources connected to transmission systems as operating synchronously with the bulk power system, implicitly relying on an existing voltage and frequency reference. Accordingly, the adopted grid-following control strategy reflects the dominant configuration currently deployed in utility-scale PV plants connected to transmission grids. While advanced control strategies such as grid-forming converters can significantly influence transient stability and post-fault dynamics, their analysis is beyond the scope of this work and is identified as an important direction for future research.

The DC/AC conversion is performed using a three-level Neutral Point Clamped (NPC) voltage source converter. The switching function of the converter is implemented with a model that is directly controlled by the reference voltage. Since the converter output voltage is 260 V, a step-up power transformer is connected downstream to match the grid voltage level. An RL filter is included at the converter output to ensure waveform quality and to protect both the grid and the converter from high-frequency components.

The parameters of the PV string and converter system are listed in Table 2. Depending on the penetration level considered in the simulations, the system is duplicated and connected in parallel to supply the required power.

Table 2. PV system parameters.

System Part	Components	Values
PV Array	Number of modules	14,700
	Modules per string	7
	Strings in parallel	2100
PV Modules	Maximum power P_{mp} (W)	414.801
	Open-circuit voltage V_{oc} (V)	85.3
	Voltage at MPP V_{mp} (V)	72.9
	Short-circuit current I_{sc} (A)	6.09
	Current at MPP I_{mp} (A)	5.69
	Cells per module	128
DC-Link	Capacitor	1.3021 F
	Voltage V_{DC}	240 V
Filters	Resistor (R)	156.06 mΩ
	Inductance (L)	4.14 mH
Transformer	Rated power P_{nom}	6 MVA
	Voltage ratio (kV) (AV/BV)	Yg 230 kV/260 V D1
	R_{cc} (p.u.)	0.0012
	X_{cc} (p.u.)	0.03

2.5. Description of the Proposed EPS

In this study, the IEEE 9-bus system [14] is modeled and analyzed using the MATLAB–Simulink® R2023b environment. Its main components include: 9 buses numbered from 1 to 9; 3 conventional generators (G1, G2, and G3) located at buses 1, 2, and 3 respectively; 3 transformers; 6 transmission lines of 100 km each; and 3 static loads located at buses 5, 6, and 8. The complex base power used for expressing the quantities in per unit is set to 100 MVA.

To perform the transient stability studies, detailed data for buses, generators and lines are required. The bus data for the test system are presented in Table 3 [10].

Table 3. Bus data of the IEEE 9-bus test System.

Bus	Bus Type	V (p.u.)	P_G (MW)	Q_G (MVAr)	P_L (MW)	Q_L (MVAr)
1	Slack	1.04	–	0	0	0
2	PV	1.025	163	0	0	0
3	PV	1.025	85	0	0	0
4	PQ	0	0	0	0	0
5	PQ	0	0	0	125	50
6	PQ	0	0	0	90	30
7	PQ	0	0	0	0	0
8	PQ	0	0	0	100	35
9	PQ	0	0	0	0	0

The slack (reference) bus has a predefined voltage magnitude and phase angle ($|V|$ and δ) of 1.04 p.u. and 0°, respectively, while its active and reactive powers are determined from the load flow analysis. The generator (PV) buses have specified voltage magnitudes ($|V|$) and active power outputs (P_g), whereas the corresponding reactive powers (Q_g) and voltage angles (δ) are obtained from the load flow results. Similarly, the remaining buses are considered as PQ (load) buses with defined real and reactive power demands, while their voltage magnitudes ($|V|$) and phase angles (δ) are derived from the same analysis. The dynamic parameters of the three synchronous generators are listed in Table 4 and the line data are detailed in Table 5 [10]. The damping coefficients of the synchronous generator models were set to zero ($D = 0$) to avoid introducing additional damping effects that could mask the influence of PV penetration on electromechanical oscillations and transient stability behavior. The per-unit system is based on a 100 MVA power base.

2.6. Methodology

In this section, we present the methodological approach adopted to model and simulate an electric power system with two different levels of PV penetration, with the objective of assessing its transient stability. This approach clearly defines the goals of the study, the tools used, and the assumptions made to ensure that the simulation remains both realistic and exploitable.

The system is modeled in MATLAB/Simulink® R2023b and is based on the IEEE 9-bus system, which includes three conventional generators, three transformers, six transmission lines of 100 km each, and three static loads. For the penetration levels, two scenarios are considered, in accordance to the following classification [23,24]:

- Moderate penetration level: 25%;
- High penetration level: 40%.

Table 4. Dynamic data of the three synchronous generators used in the IEEE 9-bus system.

Parameter	G1	G2	G3
Type	Synchronous Generator	Synchronous Generator	Synchronous Generator
Operation			
Rated Power (MVA)	512	270	125
Nominal Voltage (kV)	24	18	15.5
Power Factor	0.90	0.85	0.85
H (s)	2.6312	4.1296	4.768
D (p.u./Hz)	0	0	0
r_a (p.u.)	0	0	0
x_d (p.u.)	1.70	1.70	1.22
x_q (p.u.)	1.65	1.62	1.16
x'_d (p.u.)	0.27	0.256	0.174
x'_q (p.u.)	0.47	0.245	0.25
x''_d (p.u.)	0.20	0.185	0.134
x''_q (p.u.)	0.20	0.185	0.134
x_c (p.u.)	0.16	0.155	0.0078
T'_{d0} (s)	3.80	4.80	8.97
T'_{q0} (s)	0.48	0.50	0.50
T''_{d0} (s)	0.01	0.01	0.033
T''_{q0} (s)	0.0007	0.007	0.07
$S(1.0)$ (p.u.)	0.09	0.125	0.1026
$S(1.2)$ (p.u.)	0.40	0.45	0.432

Table 5. Transmission line data of the IEEE 9-bus system.

Line No.	From Bus	To Bus	R (p.u.)	X (p.u.)	$B/2$ (p.u.)
1	7	8	0.0085	0.072	0.0745
2	7	5	0.0320	0.161	0.1530
3	8	9	0.0119	0.1008	0.1045
4	5	4	0.0100	0.085	0.0880
5	6	4	0.0170	0.092	0.0790
6	9	6	0.0390	0.170	0.1790
7 (T1)	1	4	0	0.0576	0
8 (T2)	2	7	0	0.0625	0
9 (T3)	3	9	0	0.0586	0

These penetration levels were selected to reflect operating conditions increasingly investigated in modern transmission systems undergoing large-scale renewable energy integration and growing shares of inverter-based generation. In particular, current transmission-level planning studies face increasing concerns regarding the impact of converter-based generation on transient stability margins, post-fault operability, and system dynamic behavior under high renewable penetration conditions [6–9]. The selected penetration levels therefore provide representative scenarios for evaluating these emerging stability and operational challenges while remaining consistent with recent transient stability studies available in the literature [10,13,14].

PV penetration is introduced directly at the buses where loads are connected, and in two configurations: a concentrated penetration at one of buses 5, 7, or 8, where the total

PV power is injected at the selected bus; and a distributed penetration across the three buses simultaneously, where the injected power is shared proportionally according to the load distribution at each bus, following Equation (12). The conventional generators are not replaced with smaller units under renewable energy penetration scenarios. Instead, their operating power is reduced to prioritize renewable energy penetration. The reduction on the PV side is also performed proportionally, following a formulation consistent with the proportionality of the load.

$$P_{G_{i,\text{new}}} = P_{G_{i,\text{ref}}} - \left(\frac{P_{G_{i,\text{ref}}}}{P_{t,\text{system}}} \right) \cdot P_{\text{PV,inj}} \tag{12}$$

where: $P_{G_{i,\text{new}}}$ is the adjusted power of generator i; $P_{G_{i,\text{ref}}}$, the power of generator i in the reference case without PV penetration; $P_{t,\text{system}}$, the total generated power in the reference system; and $P_{\text{PV,inj}}$ the total active power injected by the PV systems.

For the transient stability study, a permanent three-phase symmetrical fault is applied, as it represents the most severe type of disturbance in an electric power system [10]. A permanent fault means that the line on which the disturbance occurs is removed from service after fault clearing. The fault location is chosen on the line closest to the largest PV generator, since disturbances near large generators typically produce stronger effects. Because transient stability phenomena occur over a short duration, all simulations are performed over a 7 s window, with the fault activated at $t = 1$ s. The primary conditions of the PV system (irradiance, temperature) are assumed to remain constant during the simulation.

The Critical Clearing Time is used as the main indicator to determine the transient stability of the system by analyzing the rotor angle response of the generators following the disturbance. The CCT corresponds to the maximum duration during which a disturbance can persist without causing loss of synchronism.

A series of simulations is performed by progressively increasing the fault duration in 10 ms increments. The maximum fault duration that allows the system to remain stable is considered the CCT. This resolution was considered sufficient for the comparative evaluation of transient stability trends among the analyzed scenarios. Although a finer resolution could slightly modify the exact CCT values, it is not expected to significantly affect the relative stability comparisons presented in this study. An additional simulation is carried out using a fault duration 10 ms longer than the CCT, in order to illustrate the behavior of the unstable system. As a complementary analysis, the active power generated by the solar system is also presented to observe the dynamic response of the different sources before and after the system disturbance.

The different scenarios used for the study are considering a permanent three-phase symmetrical fault on transmission line 7–5 for the different levels of PV penetration determined as percentages using Equation (13) (0%, 25%, and 40%). In each case, except for the first, the penetration is applied in a concentrated manner near the static loads at buses 5, 6, and 8, and then distributed uniformly among these three buses. In this situation, the distribution of PV power follows the same pattern as that of the static loads. These same scenarios were simulated considering a permanent three-phase fault on line 9–6, which represents a distinct electrical location within the grid, in order to assess the robustness of the observed trends.

$$\text{PV penetration level} = \frac{\text{Renewable generation (MW)}}{\text{Total demand (MW)}} \tag{13}$$

Tables 6 and 7 present, respectively, the simulation modes used and the active power corresponding to the different penetration levels according to Equation (12).

Figures 3 and 4 present, respectively, the single-line diagrams of the reference model and the model constructed with distributed PV penetration at buses 5, 6, and 8 as an example.

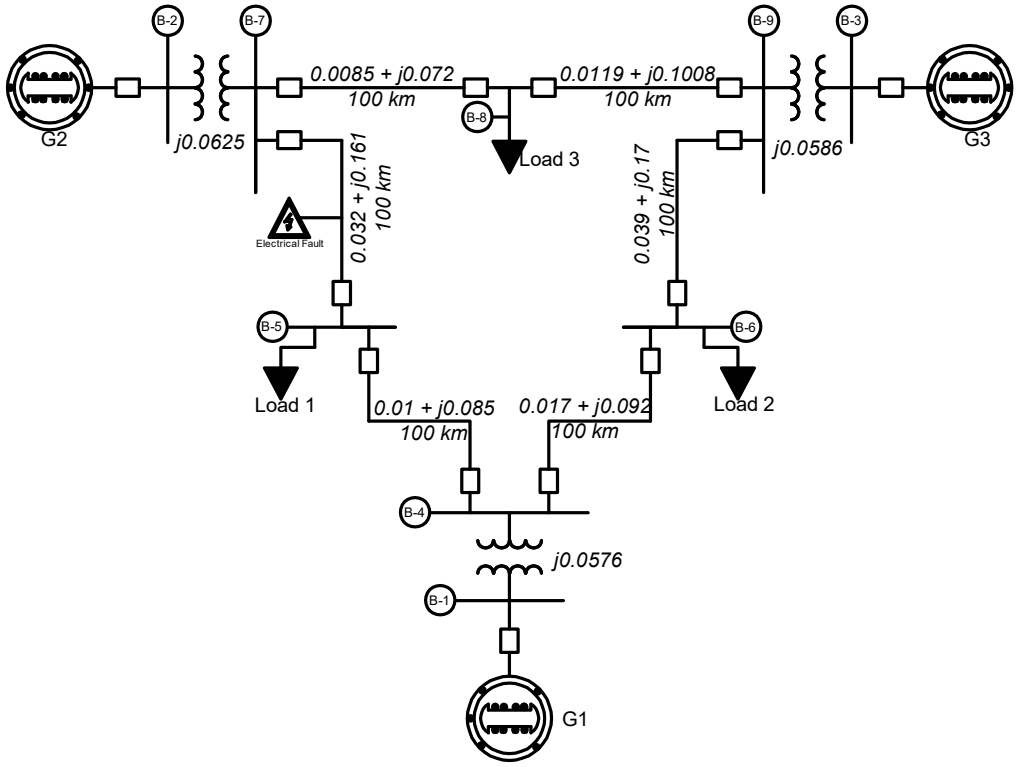


Figure 3. Single-line diagram of the 9-bus system with the fault.

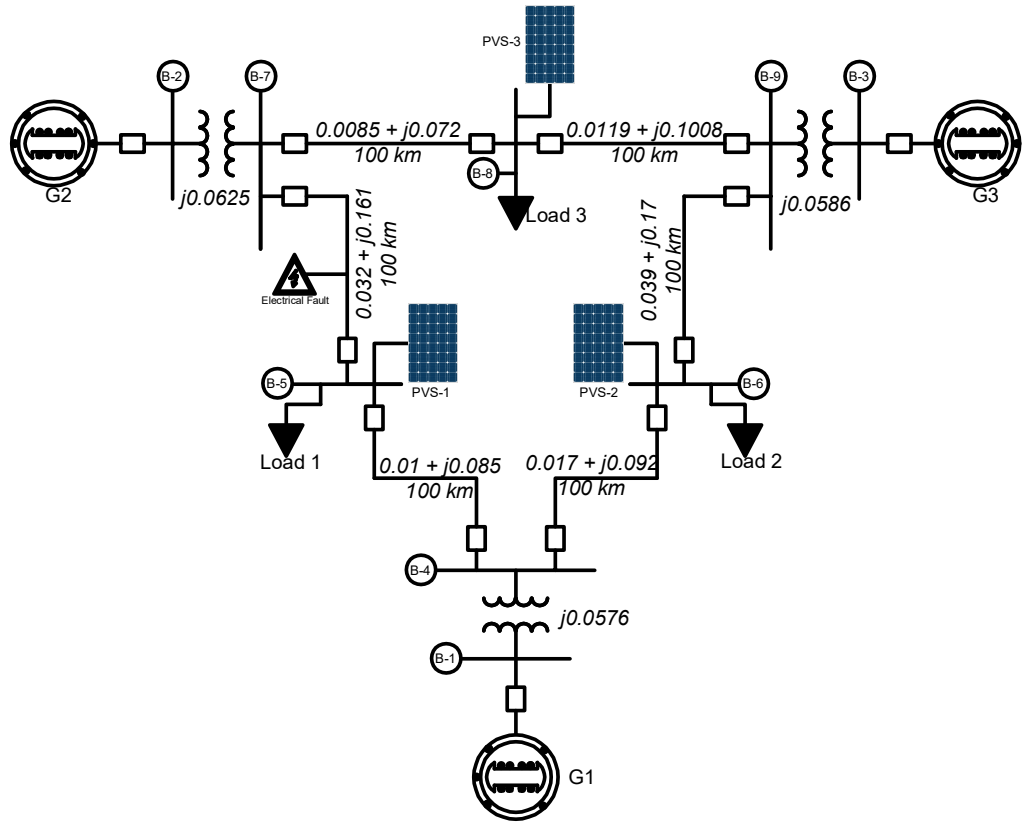


Figure 4. Single-line diagram of the 9-bus system with the fault and PV distributed across the three buses.

Table 6. Simulation modes used for each scenario.

Sources	Simulation Mode
Conventional generators	Phasor discrete mode; Sampling time: 5.0505×10^{-3} s; Solver: Ode1be
Conventional generators and PV	EMT (Electromagnetic Transients); Discrete mode; Sampling time: 5.0505×10^{-4} s; Solver: ODE23tb (or Backward Euler for higher stability).

Table 7. Active PV and adjusted conventional generation power for each penetration level.

Penetration Level	%	PV Concentrated (MW)	PV Distributed (N5/N6/N8) (MW)	G1 (MW)	G2 (MW)	G3 (MW)
Reference case	0	–	–	–	163.0	85.0
Moderate	25	79.0	31.5/22.5/25.0	–	123.5	64.5
High	40	126.0	50.0/36.0/40.0	–	100.0	52.5

3. Results and Discussion

3.1. Reference Case (0% PV)

To evaluate the transient stability of the IEEE 9-bus system, a permanent three-phase fault was applied on transmission line 7–5, following the methodology outlined in Section 2.6. The time-domain simulation shows that, for a fault duration of 210 ms, all three synchronous generators remain stable after the clearance of the disturbance. However, when the fault duration is increased to 220 ms, the system is no longer able to return to a stable post-fault operating condition.

Accordingly, the CCT of the reference case (without renewable energy penetration) is estimated at 210 ms. This value serves as the baseline for all subsequent scenarios analyzed in this study.

Figure 5 illustrates the rotor angle trajectories of the three generators. For a 210 ms fault, the rotor angles reconverge within approximately three seconds after the disturbance is cleared, indicating a stable post-fault response. In contrast, for a 220 ms fault, the rotor angles exhibit persistent oscillations and diverge with time, demonstrating a loss of synchronism and confirming instability.

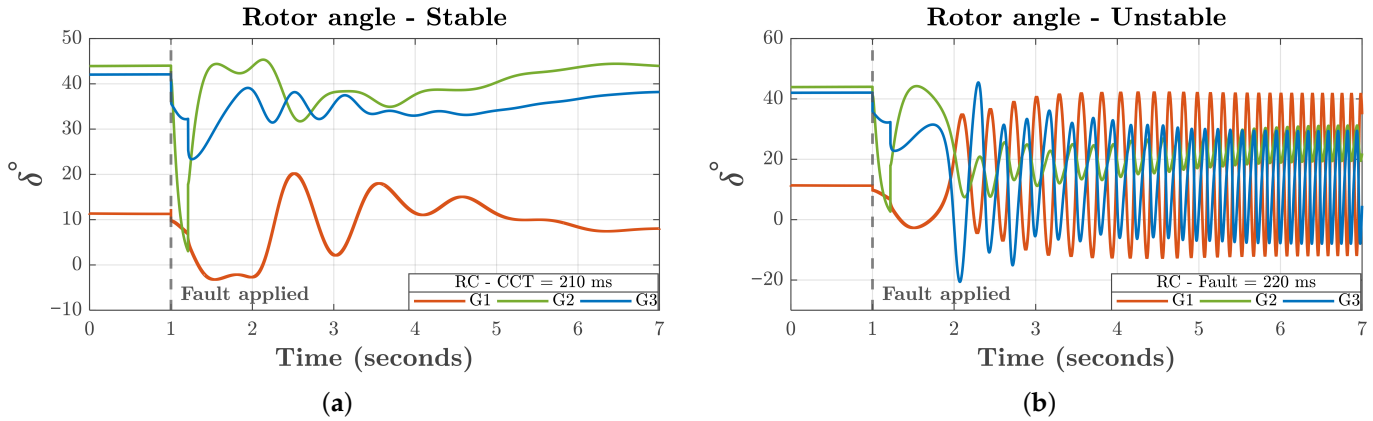


Figure 5. Rotor angle displacement of the generators: (**a**) stable condition and (**b**) unstable condition.

3.2. Impact of PV Penetration on the CCT

As described in Section 2.6, the same permanent three-phase fault is applied to the modified power system for all PV penetration levels. Table 8 presents the CCT values

obtained for each simulated scenario, illustrating the impact of PV penetration on the transient stability of the system.

Table 8. Critical Clearing Time for concentrated and distributed PV at penetration levels of 25% and 40%.

Penetration Scenario	CCT (25%) [ms]	CCT (40%) [ms]
PV at Bus 5	440	1080
PV at Bus 6	410	1130
PV at Bus 8	290	650
Distributed (5/6/8)	340	1020

In general, PV penetration has a positive impact on the CCT for all penetration levels and topologies, as long as the synchronous generators remain in service and the system inertia is preserved. The increase in CCT values is explained by the reduction in the mechanical power supplied by each synchronous generator, which decreases the rotor acceleration during the fault $(P_m - P_e)$. As a result, the rotor angle δ evolves more slowly, allowing the system to withstand longer fault durations before losing synchronism.

Although the overall effect is positive, the penetration location also plays an important role in determining system robustness. For concentrated penetrations, PV penetration at bus 8 consistently yields the lowest CCT values, regardless of the penetration level (see lines 1–3 in Table 8). This can be attributed to the fact that bus 8 is electrically the farthest from the slack bus, leading to weaker electromechanical synchronizing interactions with the synchronous generation sources. In other words, the higher electrical distance to the slack generator increases the sensitivity of bus 8 to rotor angle deviations during the disturbance, thereby reducing the transient stability margin.

For distributed penetrations, the robustness of the system improves (line 4 of Table 8) compared with the concentrated penetration at bus 8 (line 3). However, it remains lower than the robustness obtained when PV is concentrated at buses 5 or 6 (lines 1 and 2). This behavior can be explained by the fact that a non-negligible portion of the distributed PV power is still injected at bus 8, which continues to weaken the global synchronizing strength of the system, even though distribution mitigates part of the negative effect associated with this penetration point.

The simulations also reveal that the increase in CCT between the two penetration levels is not linear, regardless of the penetration topology. This strong variation arises because the rotor equation described in Equation (1) does not produce a linear response with respect to the mechanical power input. A reduction in P_m leads to a rapid decrease in the accelerating power $(P_m - P_e)$, which significantly modifies the stability behavior of the machine. As a result, the system shifts into a more favorable stability region, causing a disproportionate increase in CCT as PV penetration rises from 25% to 40%.

3.3. Post-Fault Dynamic Behavior

3.3.1. Rotor Angle Dynamics

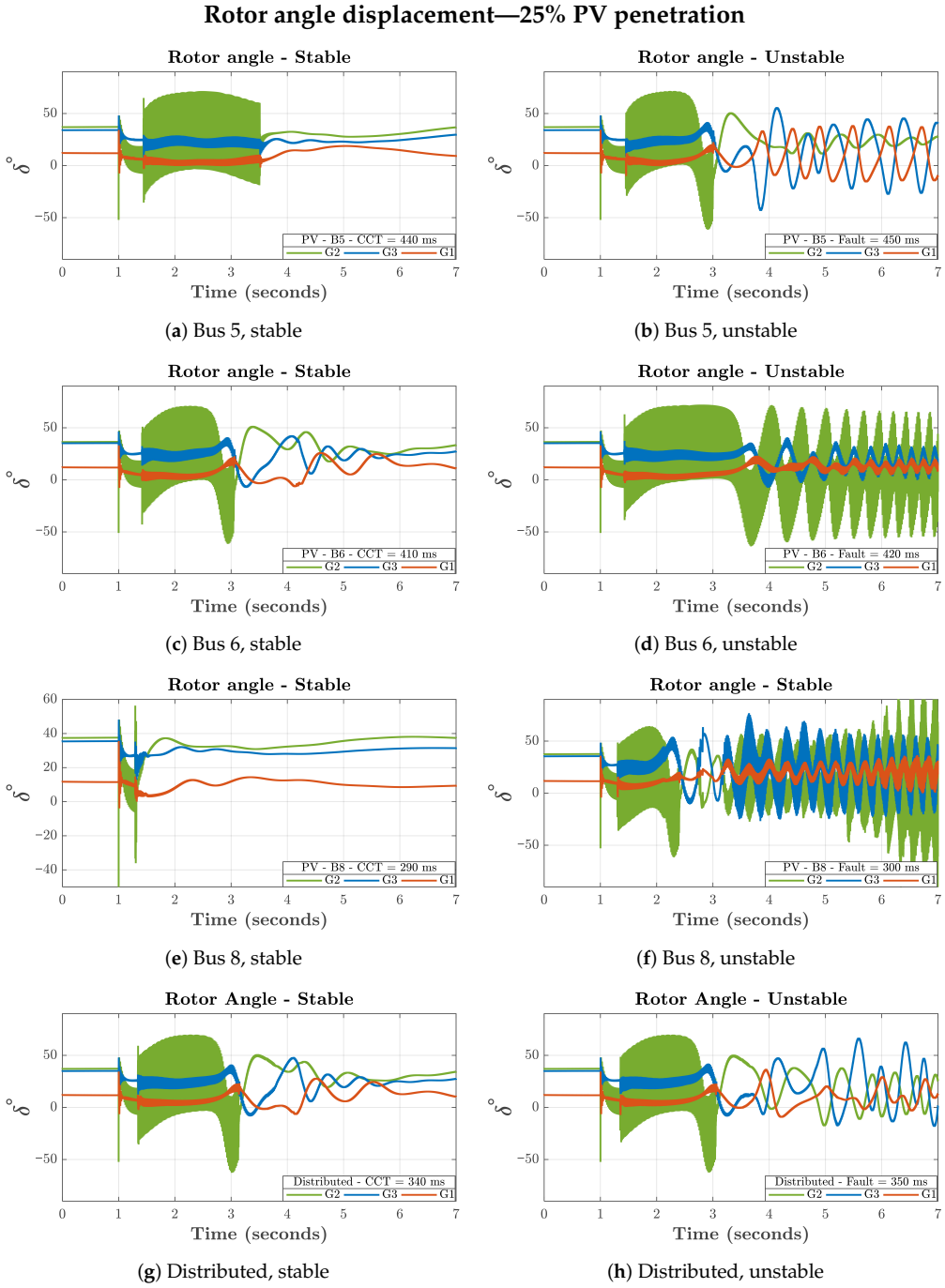
The increase in CCT values observed in the previous section suggests a more robust system when subjected to severe disturbances. However, the analysis of post-fault behaviors shows that the rotor angles exhibit oscillations of larger amplitude compared to the reference case, and of longer duration.

These prolonged oscillations are related to the converter-based nature of PV generation, which contributes less directly to the natural electromechanical synchronization mechanisms of the system. The more sustained oscillatory behavior observed under higher PV penetration levels is associated with the temporary imbalance between mechanical and

electrical power following fault clearance, leading to more pronounced oscillatory behavior and a delayed return toward synchronized operation.

Despite these more sustained oscillations and delayed recovery characteristics, these cases are still considered stable. According to the literature, for small power systems such as the IEEE 9-bus system, the rotor angles are generally expected to show a clear tendency to return toward a synchronized trajectory within approximately 3 to 5 s following fault clearance [19]. In the present study, this behavior is used as a complementary qualitative indicator of acceptable post-fault dynamic recovery.

Figures 6 and 7 illustrate the stable and unstable behaviors observed across the different simulated scenarios.



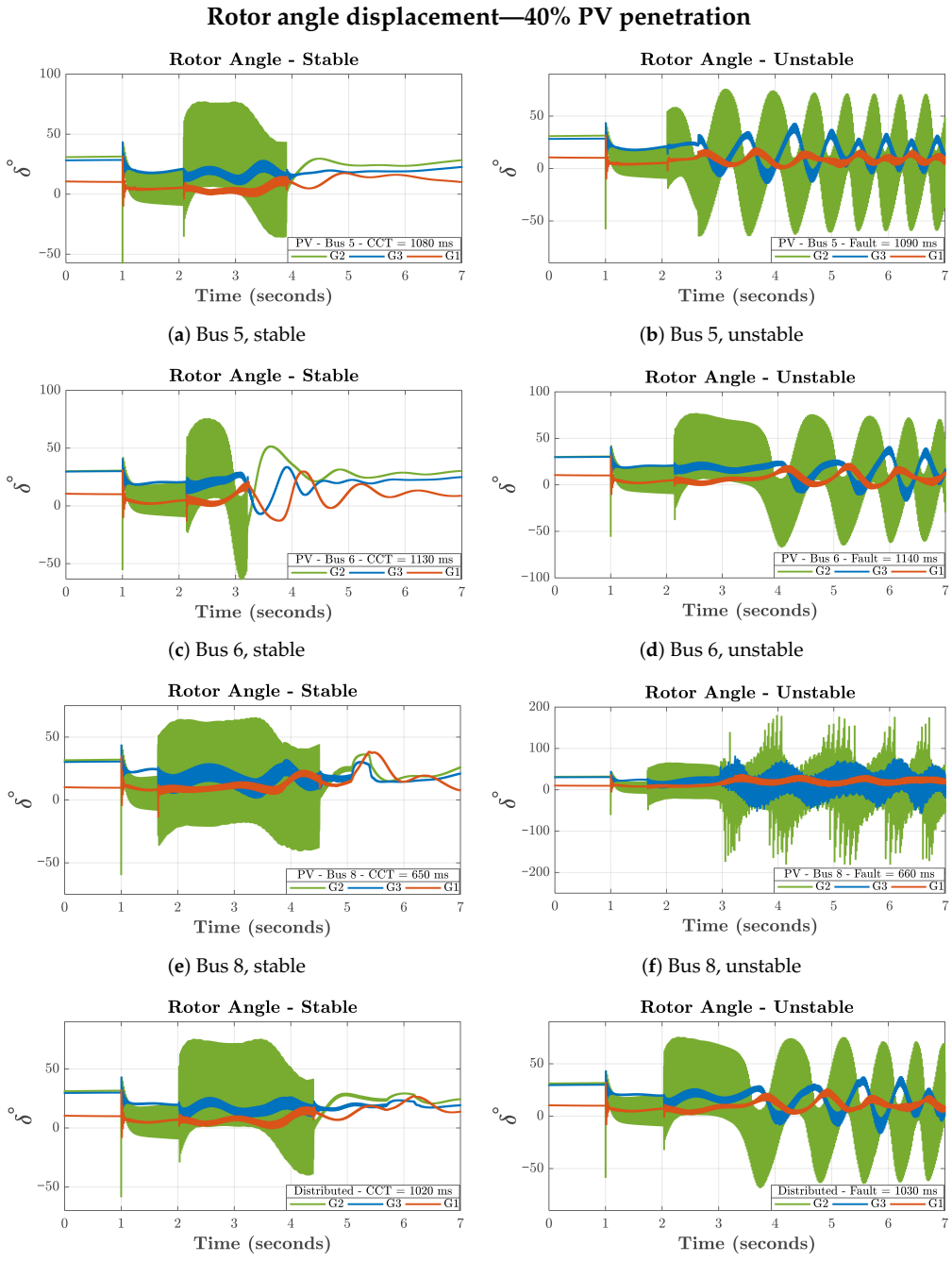
(**a**) Bus 5, stable (**b**) Bus 5, unstable

(**c**) Bus 6, stable (**d**) Bus 6, unstable

(**e**) Bus 8, stable (**f**) Bus 8, unstable

(**g**) Distributed, stable (**h**) Distributed, unstable

Figure 6. Rotor angle displacement of the generators for 25% PV penetration: stable (**a**,**c**,**e**,**g**) and unstable (**b**,**d**,**f**,**h**) for concentrated and distributed penetrations.



(**a**) Bus 5, stable (**b**) Bus 5, unstable

(**c**) Bus 6, stable (**d**) Bus 6, unstable

(**e**) Bus 8, stable (**f**) Bus 8, unstable

(**g**) Distributed, stable (**h**) Distributed, unstable

Figure 7. Rotor angle displacement of the generators for 40% PV penetration: stable (**a**,**c**,**e**,**g**) and unstable (**b**,**d**,**f**,**h**) for concentrated and distributed penetrations.

3.3.2. Active Power Dynamics

The analysis of active power provides a key indicator of the system's operational capability following a disturbance. Among the existing standards governing the interconnection of renewable energy sources to the electric grid, IEEE 1547-2018 and IEEE 2800-2022 specify that renewable energy sources should not disconnect unnecessarily and must support the grid during and after a disturbance [11,12]. This section examines the obtained results to assess compliance with these requirements. In the present study, the post-fault active power recovery behavior is qualitatively evaluated according to the general recovery expectations described in these standards. Table 9 summarizes the main recovery behaviors considered in the analysis.

Table 9. General recovery behaviors considered based on IEEE standards.

Standard	Recovery Behavior Considered in This Study
IEEE 1547-2018	Recovery of active power following fault clearance and voltage restoration.
IEEE 2800-2022	Acceptable post-fault active power restoration capability of inverter-based resources.

25% PV Penetration

Concentrated penetrations:

- **Bus 5:** The active power exhibits oscillations after fault clearing and stabilizes within approximately 2 s, meeting the normative requirements.
- **Bus 6:** The power also oscillates but fails to reach 90% of its nominal value within the 2 s required by the standards, representing an operability issue.
- **Bus 8:** The injected power stabilizes immediately after fault clearing.

In all three cases, the PV system remains connected, in accordance with LVRT requirements. The observed oscillations are primarily driven by the dynamics of synchronous generators, as PV inverters operate in grid-following mode.

Distributed penetration: The active power injected at buses 5 and 6 shows behavior similar to that of the concentrated cases. However, at bus 8, the power does not stabilize within the required time window, also indicating a lack of operational compliance. With two out of three sites failing to meet the requirements, the system exhibits operability limitations for this level of distributed penetration.

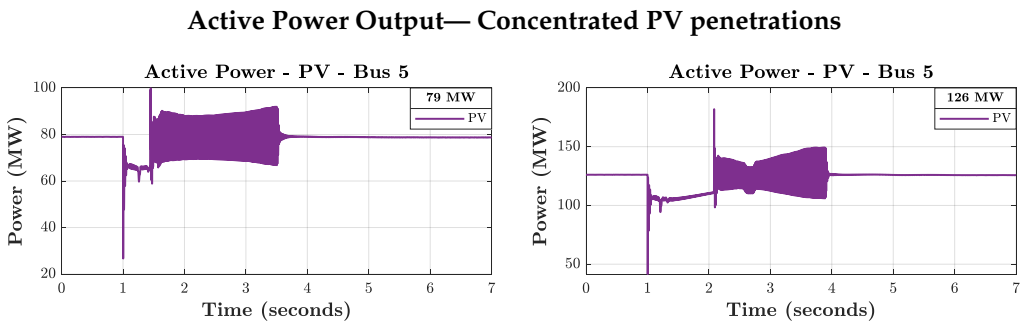
40% PV Penetration

Concentrated penetrations:

- **Bus 5 and Bus 6:** Active power oscillates after the disturbance but stabilizes within the required timeframe.
- **Bus 8:** Oscillations persist and eventually lead to loss of synchronism and disconnection, highlighting a major operability issue.

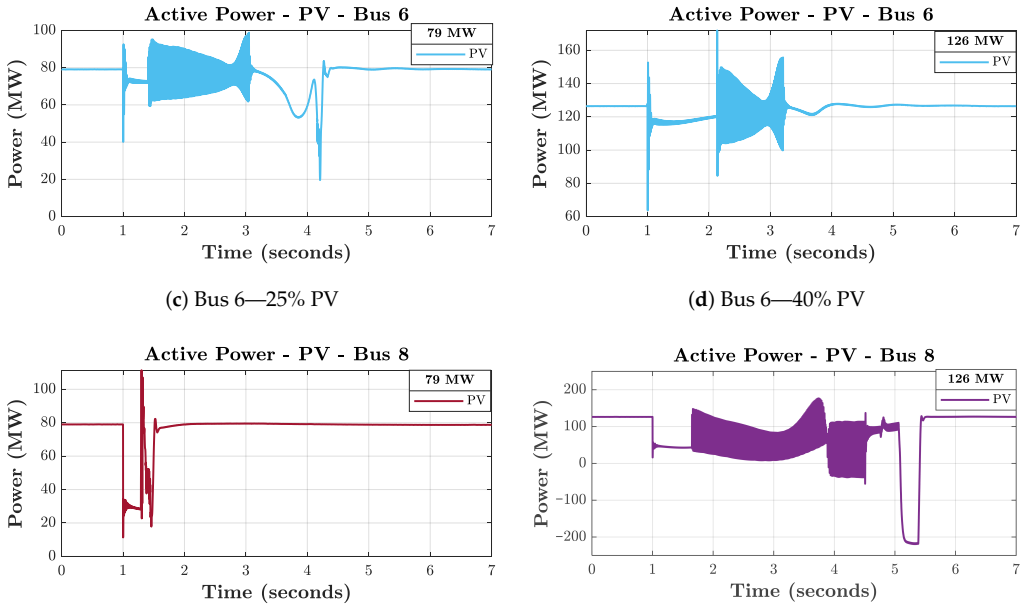
Distributed penetration: All three penetration sites exhibit non-compliant dynamic behavior relative to the normative criteria, indicating that the system is unable to satisfy operability requirements at this penetration level.

Figures 8 and 9 illustrate the evolution of the PV active power for all simulated cases.



(**a**) Bus 5—25% PV (**b**) Bus 5—40% PV

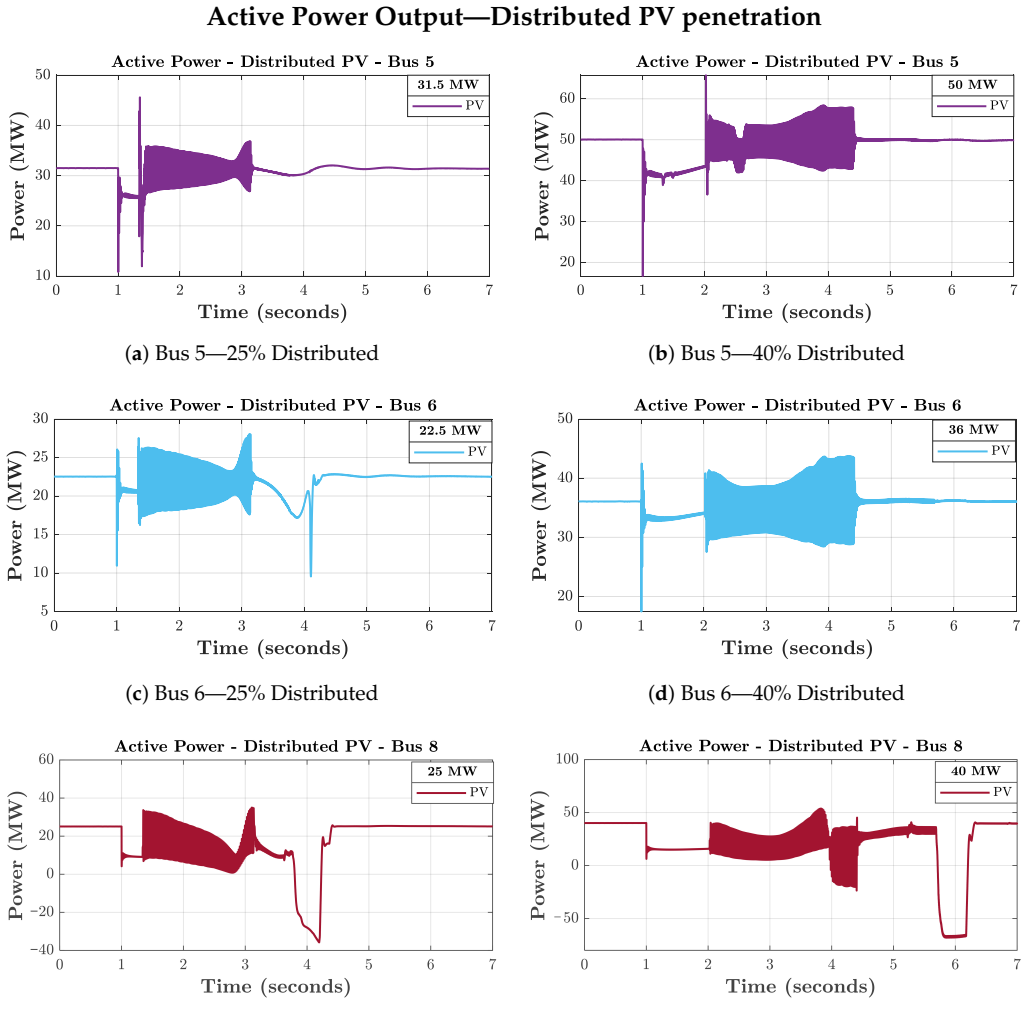
Figure 8. *Cont.*



(**c**) Bus 6—25% PV (**d**) Bus 6—40% PV

(**e**) Bus 8—25% PV (**f**) Bus 8—40% PV

Figure 8. Active power response of PV systems for concentrated penetrations under 25% and 40% penetration levels.



(**a**) Bus 5—25% Distributed (**b**) Bus 5—40% Distributed

(**c**) Bus 6—25% Distributed (**d**) Bus 6—40% Distributed

(**e**) Bus 8—25% Distributed (**f**) Bus 8—40% Distributed

Figure 9. Active power response of distributed PV systems for 25% and 40% penetration levels across buses 5, 6, and 8.

3.4. Effect of Fault Location on Transient Stability

3.4.1. Impact on CCT

Table 10 presents the CCT values obtained for a permanent three-phase fault on line 9–6, alongside those previously determined for the fault on line 7–5, for all simulated penetration scenarios.

Table 10. Comparative Critical Clearing Time values for faults on lines 7–5 and 9–6, at PV penetration levels of 25% and 40%.

	Fault on Line 7–5 [ms]		**Fault on Line 9–6 [ms]**	
Reference Case	**210**		**340**	
Penetration Scenario	**CCT (25%)**	**CCT (40%)**	**CCT (25%)**	**CCT (40%)**
PV at Bus 5	440	1080	590	1340
PV at Bus 6	410	1130	540	1200
PV at Bus 8	290	650	490	610
Distributed (5/6/8)	340	1020	580	1210

The reference case yields a higher CCT for the fault on line 9–6 (340 ms) compared to line 7–5 (210 ms). This difference can be attributed to the electrical proximity of line 9–6 to the smallest generator in the grid (G3), which reduces the rotor acceleration during the fault ($P_m - P_e$), thereby allowing the system to withstand longer fault durations before losing synchronism.

For both penetration levels, the same trend observed in the original contingency is confirmed: the CCT increases with rising PV penetration with respect to the reference case, regardless of the fault location. Furthermore, for a given penetration scenario, the system consistently exhibits higher CCT values when the fault occurs on line 9–6, indicating greater robustness under this contingency. Nevertheless, regardless of the fault location, PV penetration at bus 8 consistently yields the lowest CCT values among all concentrated penetration scenarios. This confirms that bus 8 represents the most critical integration point in the grid for transient stability, independently of the fault location considered.

3.4.2. Post-Fault Dynamic Behavior

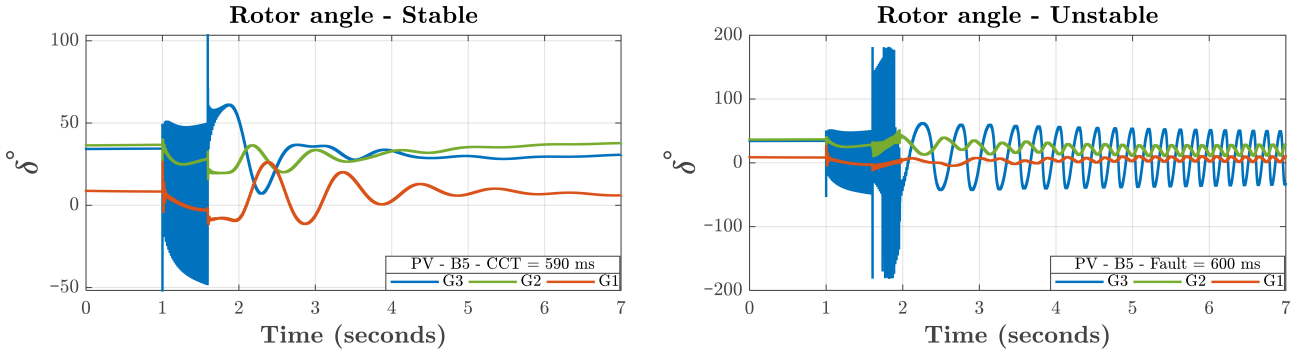
Rotor Angle Dynamics

For the fault on line 9–6, the post-fault rotor angle dynamics are generally more favorable from the transient stability perspective than those observed for the fault on line 7–5. The oscillations are of smaller amplitude and damp out more rapidly across all scenarios, consistent with the higher CCT values reported in Table 10. In all stable cases, the rotor angles reconverge toward a synchronized trajectory within the 3 to 5 s window [19], confirming transient stability under this contingency. This improvement is illustrated in Figure 10, which shows the stable and unstable rotor angle trajectories for Bus 5 at 25% PV penetration, where the reduced oscillation amplitude is clearly visible compared to the corresponding case for the fault on line 7–5 (Figure 6).

Active Power Dynamics

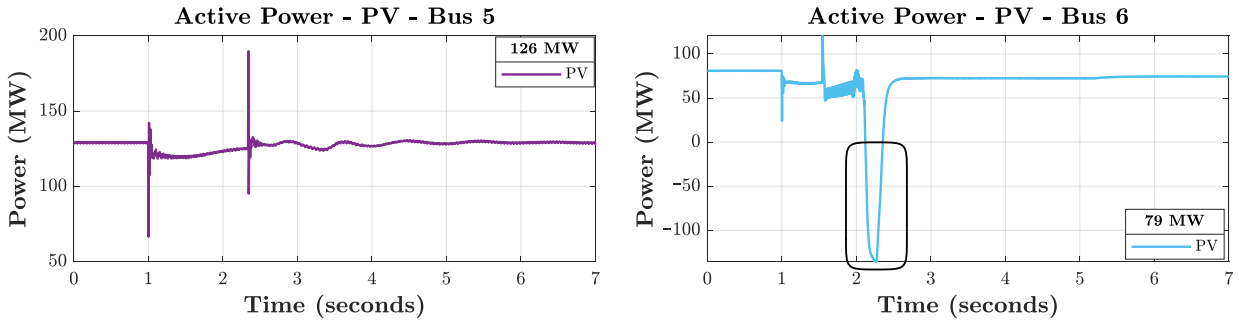
Despite the improved rotor angle behavior, the active power analysis reveals significant operability concerns. Six out of eight penetration scenarios do not meet the recovery requirements of IEEE 1547-2018 and IEEE 2800-2022, compared to four out of eight for the fault on line 7–5. In both penetration levels, Bus 5 remains the only compliant scenario, as illustrated in Figure 11 for 40% PV penetration, where the active power stabilizes within the required timeframe. In contrast, penetrations at Bus 6, Bus 8, and the distributed configuration consistently fail to restore active power within the normative time window, as

shown in Figure 11 for Bus 6 at 25% penetration. These results confirm the trend observed for the fault on line 7–5 and highlight that a higher CCT does not guarantee operational compliance: both transient stability margins and post-fault active power recovery must be jointly considered when planning PV integration into the grid.



(**a**) (**b**)

Figure 10. Rotor angle displacement of the generators for 25% PV penetration under fault on line 9–6: (**a**) Bus 5, stable; (**b**) Bus 5, unstable.



(**a**) (**b**)

Figure 11. Active power response of PV systems under fault on line 9–6: (**a**) Bus 5 at 40% penetration and (**b**) Bus 6 at 25% penetration. The highlighted region in (**b**) indicates a temporary negative active power response, meaning that power flows from the grid toward the PV system during the post-fault recovery period, which is considered non-compliant with expected operational behavior.

4. Comparison with Related Studies

This section analyzes the key findings on transient stability in the standard IEEE 9-bus test system (WSCC system) under high PV penetration. Inverter-based PV penetration transforms the system dynamics, traditionally dominated by synchronous machines, and presents a dual impact: it improves stability at moderate levels but deteriorates system response by reducing rotational inertia when conventional synchronous generators are displaced. However, differences in converter control strategies and dynamic modeling approaches may also contribute to the disparities observed among previous studies.

The main conclusions are as follows:

1. Eftekharnejad et al. [9] examined the impact of high PV penetration levels (up to 50%) on both steady-state and transient stability of a large interconnected transmission system representing a portion of the Western U.S. interconnection. In their study, PV systems replace a portion of conventional generation, resulting in a reduction in system inertia. Under these conditions, the authors report both detrimental and beneficial impacts depending on the penetration level and fault location, with higher penetration levels generally leading to reduced CCT values and increased power oscillations. While the influence of grid topology, fault location, and disturbance

type on system stability is consistent with the findings of the present study, the observed trend regarding CCT differs. This divergence is directly attributable to the methodological difference: in the present work, synchronous generators are not replaced, and system inertia is intentionally kept constant. Under this condition, the reduction in mechanical power output of synchronous machines leads to an increase in CCT, as demonstrated in Table 10. This comparison highlights that the impact of PV penetration on transient stability is strongly conditioned by whether or not synchronous inertia is preserved, a finding that underscores the importance of clearly distinguishing between these two integration scenarios in power system planning.

2. Sharma et al. [13] studied the impact of PV systems on the transient stability of an electric power system using indicators such as rotor speed deviation, oscillation time, and terminal voltage. The study considered two types of faults: line-to-ground and load switching. Among the most important findings: (i) stability indicators (rotor speed deviation and oscillation duration) increase with rising PV penetration level—for 5% PV penetration, the rotor speed deviation was 0.0035 and oscillation duration 432, while for 42.84% penetration these values reached 0.018 and 7.5, respectively; (ii) regarding rotor angle, transient stability decreases with increasing PV penetration, with maximum rotor angles observed at penetration levels of 14.3% and 42.84%; (iii) terminal voltage shows considerable drops or rises as PV penetration increases, due to the reduction in system inertia caused by the displacement of centralized generation; and (iv) electrical frequency deviation increases with PV penetration level, due to the reduction in stored kinetic energy as conventional generation units are reduced. Similarly to Eftekharnejad et al. [9], the results of Sharma et al. [13] are obtained under conditions where synchronous generators are partially replaced by PV generation, leading to inertia reduction. This methodological difference explains the apparent contradiction with the present study: while Sharma et al. report that the system loses stability beyond 40% PV penetration due to inertia reduction, our results show an increase in CCT at the same penetration level, precisely because synchronous inertia is intentionally maintained constant. This comparison further reinforces that inertia preservation is the key factor determining whether high PV penetration improves or deteriorates transient stability margins.
3. Loji et al. [14] investigated the impact of increasing PV penetration on the transient stability of the IEEE 9-bus system using DigSILENT PowerFactory, considering a three-phase fault applied at different locations and progressively increasing PV penetration levels up to 50%. Transient stability was assessed through the relative rotor angle deviation with respect to the reference generator and the CCT. Among the key findings, the authors report that the system exhibits maximum rotor angle deviations under fault conditions, with oscillations between G2 and G3 that do not damp out, indicating deteriorated transient stability. Furthermore, the system remains dynamically stable for penetration levels slightly below 50% and becomes unstable beyond this threshold. The observations regarding fault location sensitivity are consistent with the findings of the present study: transient stability is severely affected under fault conditions in PV-integrated grids, and the proximity of the fault to the PV source worsens system behavior. These findings also align with the identification of Bus 8 as the most critical integration point in the present work, as it represents the bus electrically farthest from the slack generator, making it more sensitive to rotor angle deviations during disturbances.
4. Kamel et al. [10] examined: (i) the effects of PV penetration levels; (ii) the location of PV systems; (iii) the type of faults (symmetrical vs. asymmetrical, permanent vs. temporary); and (iv) the reduction in inertia of conventional synchronous generators

on the transient stability of the electric power system. CCT was used as the main transient stability indicator. The key findings are as follows:

- **PV location (concentrated vs. distributed):** Considering a 30% PV penetration level, the main difference between distributed and concentrated PV generation was observed in the CCT values. The system was more stable when concentrated PV generation was located at buses 5 and 6, compared to the distributed case, but stability worsened when concentrated PV was located at bus 8. These results are consistent with those obtained in the present study, confirming that distributed PV generation is preferable as it provides stability improvement regardless of fault location and type.
- **Fault type:** Kamel et al. [10] compared symmetrical and asymmetrical faults, considering single-phase-to-ground faults. The study concludes that the system is more stable under asymmetrical faults, even at high PV penetration levels (30%). This is because: (i) for symmetrical (three-phase) faults, the voltages of all three phases drop practically to zero, causing the electrical power supplied to also drop to zero, which rapidly accelerates synchronous generators toward instability; and (ii) for asymmetrical faults, generator acceleration is lower, allowing stabilization under certain operating conditions. These findings are consistent with those of the present study.
- **Reduction in synchronous generator inertia:** The H values and rated power of the three synchronous machines were reduced by the same percentage as the PV penetration levels. Simulations were performed with three-phase faults on lines 5–7 and 4–5 under both distributed and concentrated PV generation. The results confirm that inertia reduction decreases CCT values and therefore system stability. This is consistent with the findings of the present study, where it is shown that when a fault occurs near a low-inertia generator, the system tends to become more unstable than when the fault occurs near a higher-inertia generator. Furthermore, it is concluded that (i) for faults on line 5–7 and (ii) for faults on line 4–5 near bus 4, inertia reduction decreased CCT values compared to the constant inertia case. However, faults at this location presented higher CCT values compared to faults of the same type on line 5–7. These results are consistent with those obtained in the present study, as unequal inertia distribution and fault location significantly influence the transient stability performance of electric power systems.

The main findings from the literature compared to those of the present study are summarized in Table 11.

Table 11. Comparison of transient stability studies under PV penetration in IEEE benchmark systems.

Test Model	Penetration Level (%)	Fault Type	Fault Location	Indicator	Software	Main Findings	Ref.
IEEE 22-bus	10, 20, 30, 40 and 50	Three-phase fault	Buses 1569, 886/1164, 913	–	PSAT, DSATools (PowerTech Labs)	PV systems present both negative and positive impacts on transient stability, depending on the size and connection type of distributed generation, as well as the type and location of transients.	[9]
IEEE 9-bus	14.3, 28.6 and 42.85	Line-to-ground fault	Line 7–5	Rotor speed, deviation, oscillation duration, terminal voltage, frequency deviation	DigSILENT™ PowerFactory	The closer the fault to the PV system, the worse the transient stability. System stability is lost beyond 40% PV penetration due to inertia reduction caused by displacement of synchronous generators.	[13]

Table 11. *Cont.*

Test Model	Penetration Level (%)	Fault Type	Fault Location	Indicator	Software	Main Findings	Ref.
IEEE 9-bus	10, 40, 50, and 100	Three-phase fault	Bus 5	CCT, rotor angle, deviation	DigSILENT™ PowerFactory	Transient stability is severely affected under fault conditions, and more severely as the fault gets closer to the PV source. Stability worsens as PV penetration increases for a given fault location.	[14]
IEEE 9-bus	10, 20 and 30	Symmetrical and asymmetrical	Lines 7–5 and 4-5	CCT	PowerWorld® Simulator	Higher PV penetration increases CCT when synchronous generators are not replaced. The system is more stable under asymmetrical faults. Inertia reduction decreases CCT and system stability.	[10]
IEEE 9-bus	25 and 40	Symmetrical (three-phase)	Lines 7–5 and 9–6	CCT, rotor angle, dynamics, active power recovery	MATLAB/ Simulink® R2023b	High PV penetration increases CCT across all scenarios. Bus 8 is the most critical integration point. Overall, 75% of penetration scenarios under the secondary contingency do not meet IEEE 1547-2018 and IEEE 2800-2022 requirements, highlighting that a higher CCT does not guarantee operational compliance.	This paper

5. Conclusions

This study aimed to evaluate the impact of high PV penetration on the transient stability of the IEEE 9-bus system using MATLAB/Simulink® R2023b. The results showed that, in terms of transient stability, PV penetration increases the CCT when synchronous inertia remains constant. The penetration location and topology strongly influence system robustness, with Bus 8 identified as the most critical penetration point for all penetration levels in the analyzed IEEE 9-bus configuration.

The post-fault dynamic behavior exhibited rotor angle oscillations and, in some cases, operability issues, particularly when the technical requirements of IEEE 1547 and IEEE 2800 were not met. These findings highlight the importance of planning strategies that consider the PV penetration location as well as detailed post-fault behavior to ensure operational compliance of the grid.

The analysis of a second contingency, namely a permanent three-phase fault on line 9–6, confirmed the trends observed for the fault on line 7–5. For both penetration levels, the CCT increases with rising PV penetration regardless of the fault location, and Bus 8 consistently yields the lowest stability margin among all concentrated penetration scenarios. However, the active power analysis reveals that 75% of the penetration scenarios do not meet the recovery requirements of IEEE 1547-2018 and IEEE 2800-2022, a result more severe than that observed for the fault on line 7–5. Although the system remains transiently stable from the rotor angle perspective, the larger post-fault oscillations can produce significant voltage and power fluctuations during the recovery period, affecting the ability of converter-based generation to restore active power smoothly after fault clearance. These results demonstrate that improved transient stability margins do not necessarily guarantee acceptable post-fault operational behavior, highlighting the importance of jointly evaluating rotor angle stability and active power recovery when planning the integration of PV generation into the grid.

However, this study relies on a reduced IEEE 9-bus benchmark system and exclusively considers grid-following converter-based PV generation. The synchronous inertia is intentionally kept constant in order to isolate the specific impact of PV penetration level, location, and topology on transient stability indicators such as the CCT. Considering inertia reduction simultaneously would introduce additional coupled effects, making it difficult to clearly attribute the observed trends to PV integration alone. However, it

also represents an important limitation of the present study, since practical large-scale PV integration often involves the partial replacement of synchronous generation and the associated reduction in system inertia. Consequently, the results obtained in this work should not be directly generalized quantitatively compared to scenarios involving simultaneous inertia displacement.

As a result, the findings should be interpreted as indicative trends that highlight fundamental transient stability mechanisms rather than definitive conclusions directly applicable to large-scale transmission grids. In practical power systems, additional factors such as grid size, heterogeneity, and advanced converter controls may further influence system dynamics; consequently, further investigations using larger and more realistic grids, and different fault locations, as well as temporary and unbalanced fault conditions, are required for broader generalization. The inclusion of grid-forming converters could also significantly modify the observed dynamic responses by improving synchronization behavior and post-fault active power recovery under high PV penetration conditions.

Future work may include the study of hybrid PV+BESS technologies and the use of more complex benchmark grids, such as the IEEE 14-bus and IEEE 39-bus systems, to further evaluate transient stability behavior under high PV penetration and the influence of critical integration locations under different network configurations.

Author Contributions: Conceptualization, M.J.P.; methodology, M.J.P.; software, M.J.P.; validation, E.H.-M. and M.M.-M.; formal analysis, M.J.P.; investigation, M.J.P.; resources, E.H.-M., M.M.-M., R.I.-C. and O.A.J.S.; data curation, M.J.P.; writing—original draft preparation, M.J.P.; writing—review and editing, E.H.-M., G.M.-R., J.S.-J. and R.I.-C.; visualization, M.J.P.; supervision, E.H.-M., M.M.-M. and O.A.J.S.; project administration, E.H.-M. and O.A.J.S. All authors have read and agreed to the published version of the manuscript.

Funding: This research received no external funding.

Institutional Review Board Statement: Not applicable.

Informed Consent Statement: Not applicable.

Data Availability Statement: The data supporting the findings of this study are available from the corresponding author upon reasonable request.

Acknowledgments: The authors thank the Instituto de Energías Renovables (IER–UNAM), especially Omar Rodriguéz Rivera, for technical support and resources used during simulation development.

Conflicts of Interest: The authors declare no conflicts of interest. The funders had no role in the design of the study; in the collection, analyses, or interpretation of data; in the writing of the manuscript; or in the decision to publish the results.

References

1. IRENA. *Renewable Power Generation Costs in 2022*; International Renewable Energy Agency: Abu Dhabi, United Arab Emirates, 2023.
2. Pessanha, J.; Melo, A.; Caldas, R.; Falcao, D. An approach for data treatment of solar PV generation. *IEEE Lat. Am. Trans.* **2020**, *18*, 1563–1571. [CrossRef]
3. Šešok, A.; Pavić, I. Transient stability improvement of Croatian power system using FACTS. In *Proceedings of the 11th International Conference on Innovative Smart Grid Technologies—Asia (ISGT-Asia 2022)*; IEEE: Singapore, 2022. [CrossRef]
4. Lopes, J.C.; Sousa, T. Transmission system electromechanical stability analysis with high penetration of renewable generation and battery energy storage system application. *Energies* **2022**, *15*, 2060. [CrossRef]
5. Wandhare, R.G.; Agarwal, V. Novel stability enhancing control strategy for centralized PV-grid systems for smart grid applications. *IEEE Trans. Smart Grid* **2014**, *5*, 1389–1396. [CrossRef]
6. Shah, R.; Mithulananthan, N.; Bansal, R.; Ramachandaramurthy, V. A review of key power system stability challenges for large-scale PV integration. *Renew. Sustain. Energy Rev.* **2015**, *41*, 1423–1436. [CrossRef]

7. Achilles, S.; Bebic, S. *Transmission System Performance Analysis for High Penetration Photovoltaics*; Report No. SR-581-42300; National Renewable Energy Laboratory (NREL): Golden, CO, USA, 2008.
8. Tamimi, B.; Canizares, C.; Bhattacharya, K. System stability impact of large scale and distributed solar photovoltaic generation: The case of Ontario. *IEEE Trans. Sustain. Energy* **2013**, *4*, 680–688. [CrossRef]
9. Eftekhari-Nejad, S.; Vittal, V.; Heydt, G.T.; Loehr, K. Impact of increased penetration of photovoltaic generation on power system. *IEEE Trans. Power Syst.* **2013**, *28*, 893–901. [CrossRef]
10. Kamel, R.M.; Alanzi, S.S.; Hashemi, Y.M.A. Effect of photovoltaic penetration level and location on power system transient stability during symmetrical and unsymmetrical faults. *Sustain. Energy Grids Netw.* **2024**, *38*, 101322. [CrossRef]
11. *IEEE Std 1547-2018*; IEEE Standard for Interconnection and Interoperability of Distributed Energy Resources with Associated Electric Power Systems Interfaces. IEEE: New York, NY, USA, 2018.
12. *IEEE Std 2800-2022*; IEEE Standard for Interconnection and Interoperability of Inverter-Based Resources with Associated Transmission Electric Power Systems. IEEE: New York, NY, USA, 2022.
13. Sharma, R.; Singh, M.; Jain, D.K. Power System Stability Analysis with Large Penetration of Distributed Generation. In *Proceedings of the 6th IEEE Power India Conference*; IEEE: Delhi, India, 2014; pp. 1–6. [CrossRef]
14. Loji, K.; Loji, N.; Kabeya, M. Flexibility Assessment of a Solar PV Penetrated IEEE 9-Bus System Using Dynamic Transient Stability Evaluation. In *Proceedings of the 2022 IEEE PES/IAS Power Africa Conference, Kigali, Rwanda, 2–6 August 2022*; IEEE: New York, NY, USA, 2022; pp. 1–5. [CrossRef]
15. Mazhari, S.M.; Safari, N.; Chung, C.Y.; Kamwa, I. A Hybrid Fault Cluster and Thevenin Equivalent Based Framework for Rotor Angle Stability Prediction. *IEEE Trans. Power Syst.* **2018**, *33*, 5594–5603. [CrossRef]
16. Barbosa, D.M.; Kuiava, R.; Piazza, T.S. Transient Stability Constrained Optimal Power Flow Applied to Distribution System with Synchronous Generators. *IEEE Lat. Am. Trans.* **2022**, *20*, 335–343. [CrossRef]
17. Sauer, P.W.; Pai, M.A. *Power System Dynamics and Stability*; Prentice Hall: Upper Saddle River, NJ, USA, 1998.
18. Anderson, P.M.; Fouad, A.A. *Power System Control and Stability*, 2nd ed.; Wiley: Piscataway, NJ, USA, 2003.
19. Kundur, P. *Power System Stability and Control*; McGraw–Hill: New York, NY, USA, 1994.
20. Montano, J.J.; Grisales, L.F.; Tobon, A.F.; González, D. Estimation of the parameters of the mathematical model of an equivalent diode of a photovoltaic panel using a continuous genetic algorithm. *IEEE Lat. Am. Trans.* **2022**, *20*, 616–623. [CrossRef]
21. Cervellini, M.P.; Echeverria, N.I.; Antonszczuk, P.D.; Retegui, R.A.G.; Funes, M.A.; González, S.A. Optimized parameter extraction method for photovoltaic devices model. *IEEE Lat. Am. Trans.* **2016**, *14*, 1959–1965. [CrossRef]
22. Brito, M.; Alves, M.; Canesin, C. Microgrid system with emulated PV sources for parallel and intentional islanding operations. *IEEE Lat. Am. Trans.* **2020**, *18*, 1462–1469. [CrossRef]
23. De Witt, W.; García, M.; López, R. Classification of Renewable Energy Penetration Levels in Modern Power Systems. *Int. J. Renew. Energy Res.* **2021**, *11*, 987–995.
24. Muhando, B.; Keith, K.; Holdmann, G. *Power Electronics Review—Evaluation of the Ability of Inverters to Stabilize High-Penetration Wind–Diesel Systems in Diesel-Off Mode Using Simulated Components in a Test Bed Facility*; Alaska Center for Energy and Power: Fairbanks, AK, USA, 2010.

Disclaimer/Publisher's Note: The statements, opinions and data contained in all publications are solely those of the individual author(s) and contributor(s) and not of MDPI and/or the editor(s). MDPI and/or the editor(s) disclaim responsibility for any injury to people or property resulting from any ideas, methods, instructions or products referred to in the content.